Proceedings of the ASME 2010 International Design Engineering Technical Conferences & Computers and Information in Engineering Conference
IDETC/CIE 2010
August 15-18, 2010, Montreal, Quebec, Canada

DETC2010-28998

FORWARD AND INVERSE DISPLACEMENT ANALYSIS OF AN ACTUATED SPOKE WHEEL ROBOT WITH TWO SPOKES AND A TAIL CONTACT WITH THE GROUND

Ping Ren
RoMeLa: Robotics & Mechanisms Laboratory
Mechanical Engineering Department
Virginia Tech
Blacksburg, Virginia 24061, U.S.A
Email: renping@vt.edu

Dennis Hong[1]
RoMeLa: Robotics & Mechanisms Laboratory
Mechanical Engineering Department
Virginia Tech
Blacksburg, Virginia 24061, U.S.A
Email: dhong@vt.edu

ABSTRACT

Intelligent Mobility Platform with Active Spoke System (IMPASS) is a unique wheel-leg hybrid robot that can walk in unstructured environments by stretching in or out three independently actuated spokes of each wheel. The latest prototype of IMPASS has two actuated spoke wheels and one passive tail. In order to maintain its stability, the tail of the robot is designed as a rigid shell with a geometrically convex surface touching the ground. IMPASS is considered as a mechanism with variable topologies (MVTs) due to its metamorphic configurations. Its motions on the ground, such as steering, straight-line walking and other combinations, can be uniformly interpreted as a series of configuration transformations. Among all cases of its topologies, the cases with two spokes and the tail in contact with the ground possess two d.o.f and contribute the most to its ground motion. To fully understand the characteristics of such topologies, the forward and inverse displacement analysis is developed for these cases, with the polynomial equations derived. Numerical solutions from simulation are present to validate their formulation. These results lay the kinematics foundation for the motion monitoring and planning of IMPASS. It also contributes to the design optimization of the tail's surface geometry to improve its adaptability on uneven terrains.

1. INTRODUCTION

Leg-wheel hybrid robots have been drawing more attention since they have the advantages of both legs and wheels. Legged locomotion is more adaptable to a wide range of unstructured grounds but the complicated mechanism of the legs is very difficult to implement. On the other hand, wheeled locomotion is fast and efficient but it tends to be limited to relatively smooth terrain. Therefore, in order to create a walking machine that combines the benefits of both locomotion schemes, spoke wheels or similar mechanisms can be good candidates.

Previous mobile platforms that utilize spoke wheels mainly included RHex [1] and Whegs™ [2]. RHex was a compliant-legged hexapod with a simple clock-driven open-loop tripod gait. It was different from other mobile robots in that each of its legs rotated in full circles acting as a single spoke wheel. The Whegs™ series of robots was the other derivation of the spoke wheel concept that utilized compliant tri-spoke configuration in each wheel.

The Intelligent Mobility Platform with Active Spoke System (IMPASS) robot, initially proposed in Ref. [3,4], also adopts the concept of actuated spoke wheels. Compared with preceding spoke wheel robots, the uniqueness of IMPASS mainly lies on the novel mechanism of its spoke wheels (six spokes per wheel unit, compared to three for Whegs™ and only one for RHex) and its ability to stretch each spoke in or out intelligently. The latest IMPASS prototype demonstrated in Figure 1 has two actuated spoke wheels and one passive tail. The compliant spokes are made of carbon fibers and set 60 degrees from each other. The body is covered with a carbon fiber shell. The shell has a tail, with its lower portion designed as a convex surface. As the robot walks on various terrains, climb up steps and so on, the tail, together with the spokes that contact the ground can provide a support region to maintain its stability.

[1] Address all correspondence to this author.

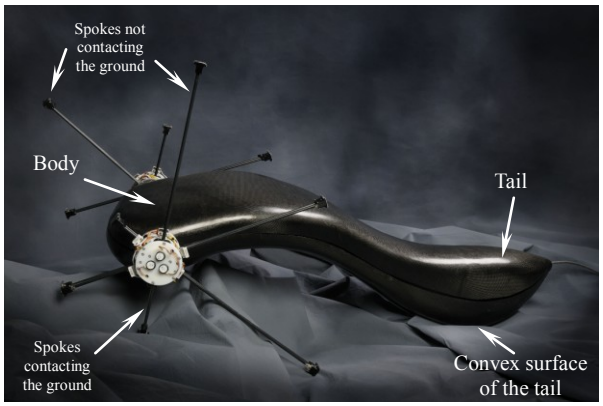

Figure 1 The prototype of IMPASS

As IMPASS moves on smooth surfaces, its body is always connected to the ground through multiple actuated spokes. By treating the ground as the base and the spokes as the limbs, this particular mobile robot can be modeled as a mechanism with variable topologies (MVTs), with each of its topological structures characterized by the contact scheme of the spokes. The variable mobility, i.e. the metamorphic degrees of freedom of the robot's body, was firstly investigated in Ref. [5] for all its topologies. Then, in the follow-up Ref. [6], it was revealed that the motions of IMPASS on the ground, such as straight-line walking, steering and other combinations, could be uniformly interpreted as a series of topological transformations.

Among all cases of its topologies, the cases with two spokes and the tail in contact with the ground possess two d.o.f and contribute the most to its locomotion. This paper is intended to address the forward and inverse kinematics in such cases in order to fully understand their topological characteristics. The content of the paper is organized as: the kinematic model of IMPASS with two spoke wheels and one tail is introduced in Section 2; followed by the forward and inverse kinematics analyses in Section 3 and 4 respectively. In Section 5, numerical solutions from simulations are presented and discussed. Finally, conclusions are drawn and future research is briefly discussed in Section 6.

2. KINEMATIC MODEL

The characteristic geometry of the IMPASS prototype in Figure 1 is extracted, and represented with the kinematic model shown in Figure 2. In this model, two spokes from the left and right wheel respectively and the tail are contacting the smooth ground. To make the presentation clear, the contacting and un-contacting spokes are represented with solid and transparent cylinders respectively. The two spoke wheels are connected with an axle. The actuation of this robot is the rotation of the spoke wheels about the axle in the direction indicated by the double arrow in this figure, and the translations of the contacting spokes through the hub of the wheel. In order to eliminate slip or bounce that could occur at the contact tips of the spokes, the two spoke wheels are constrained to rotate in the same phase and when the contacting spokes stretch in or out, their contact points with the ground must be kept stationary. The un-contacting spokes can also stretch in or out locally, but their displacements do not affect the configuration of the robot in its current topology, unless they touch the ground thus changing its topology.

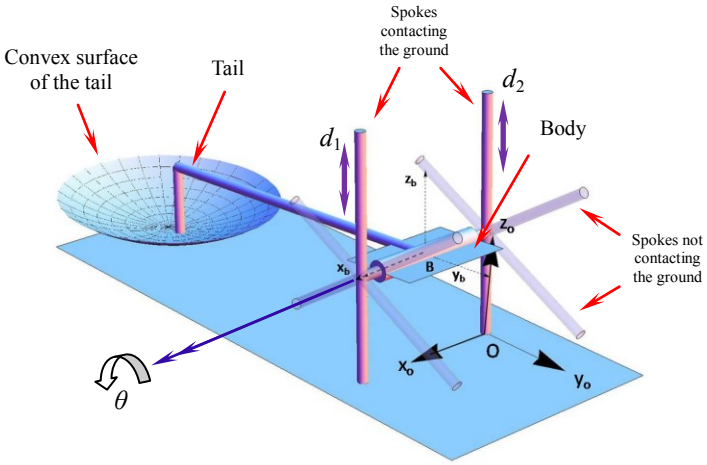

Figure 2 Kinematic model of IMPASS with two spokes and the tail in contact with the smooth ground

The geometry of the body and tail in Figure 1 is simplified, and represented with a rectangle plane connecting to a convex surface through a rigid link, as is shown in Figure 2. At present, the convex surface of the tail is designed as part of a spherical surface. The body and the tail are attached to the axle that connects the two spoke wheels. As IMPASS takes steps on the smooth ground, its tail passively touches the ground. Therefore, at any instant, there exist at least three contact points between IMPASS and the ground (two come from the contact spokes and one could come from the tail), thus providing a support region to maintain the robot's stability.

3. FORWARD KINEMATICS ANALYSIS

Forward kinematics analysis aims to calculate the position and orientation of the robot's body with given joint displacements. As for the topology of IMPASS shown in Figure 2, the joint variables that can be specified are the angular displacement of the two spoke wheels and the linear displacement of the two contacting spokes. Since the rotation of the two wheels is in phase and the translations of the two spokes are dependent on each other, there are two d.o.f in this topology.

Given the presumption that three non-collinear contact points exist, the forward kinematics of IMPASS with two spokes and the tail in contact with the ground can be formulated with the follows procedures.

First, as shown in Figure 2, two coordinate systems are established with $\{x_o, y_o, z_o\}$ fixed on the ground and $\{x_b, y_b, z_b\}$ attached to IMPASS' body. The origin O of $\{x_o, y_o, z_o\}$ is chosen at the contact point between the left spoke and the

ground, with x_o axis pointing to the right contact point and z_o axis normal to the ground. The origin B of $\{x_b, y_b, z_b\}$ is set at the midpoint of the axle, with x_b axis pointing to the right wheel center, also the direction of the spoke wheels' rotation, and y_b axis lying in the rectangle plane and pointing to the front of the body.

Secondly, assume the body coordinate system $\{x_b, y_b, z_b\}$ is positioned at the global origin with zero orientation, then with given joint displacements, the position vectors of the contact points of the two spokes ($\mathbf{P}_1$ and $\mathbf{P}_2$) with respect to the body frame can be determined using homogenous coordinates and transformation matrices as follows:

$$\begin{bmatrix} \mathbf{P}_1 \\ 1 \end{bmatrix} = R_x(\theta) \begin{bmatrix} \mathbf{p}_1 \\ 1 \end{bmatrix} \tag{1}$$

and

$$\begin{bmatrix} \mathbf{P}_2 \\ 1 \end{bmatrix} = R_x(\theta) \begin{bmatrix} \mathbf{p}_2 \\ 1 \end{bmatrix} \tag{2}$$

where

$$R_x(\theta) = \begin{bmatrix} 1 & 0 & 0 & 0 \\ 0 & \cos\theta & \sin\theta & 0 \\ 0 & -\sin\theta & \cos\theta & 0 \\ 0 & 0 & 0 & 1 \end{bmatrix} \tag{3}$$

$$\mathbf{p}_1 = \begin{bmatrix} l/2 & 0 & -d_1 \end{bmatrix}^{\mathrm{T}}$$

$$\mathbf{p}_2 = \begin{bmatrix} -l/2 & 0 & -d_2 \end{bmatrix}^{\mathrm{T}}$$

In Eqs.(1-3), l is the length of the axle; θ is the angular displacement of the two spoke wheels; d_1 and d_2 are the linear displacements of the two contacting spokes respectively, measured from the centers of the wheels to the contact points. Since the contacting spokes of the kinematic model in Figure 2 are parallel, d_1 and d_2 must obey the following constraint:

$$d_1 - d_2 = \Delta d \tag{4}$$

where Δd is a constant. This constraint is to ensure that the distance between the two spoke contact points is constant in its current topology, such that slip or bounce does not occur at the spoke tips.

If the contacting spokes are two skew spokes set 60 degrees apart rather than parallel, then Eq.(2) just needs to be modified as:

$$\begin{bmatrix} \mathbf{P}_2 \\ 1 \end{bmatrix} = R_x(\theta + \pi/3) \begin{bmatrix} \mathbf{p}_2 \\ 1 \end{bmatrix} \tag{2}*$$

and d_1, d_2 should follow the quadratic constraint instead as:

$$d_1^2 - d_1 d_2 + d_2^2 = e^2 - l^2 \tag{4}*$$

where e is the distance between the two contact points, l is again the length of the axle and both of them are constants. The detailed derivation of Eq.(4)* and discussions on the skew contact case can be found in Ref.[7].

The third contact point P_3 is due to the tail's passive touching with the smooth ground. Since the lower portion of the tail is part of a spherical surface, the contact point is actually the tangential point between the spherical surface and the ground plane. To elaborate this, assume the shell of the tail and the ground are both rigid, then the two rigid bodies contacting at a point form a *surface contact pair*, which was introduced in Ref. [8]. The surface contact pair is illustrated in Figure 3 as follows. It is a higher pair with five d.o.f.

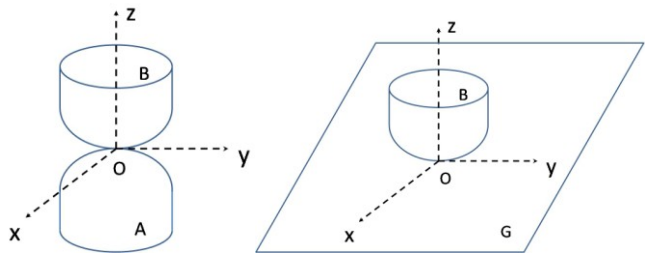

(a) (b)

Figure 3 Surface contact pair

As shown in Figure 3(a), rigid body B contacts rigid body A at point O, where the two contacting surfaces are free to roll and slide with respect to one another as long as the contact point is maintained. Replacing body A with plane G and assuming G is stationary, the case in Figure 3(b) becomes another surface contact pair in which body B can slide along plane G and rotate in three directions about point O. Therefore, the contacting case of the tail and the ground in Figure 2 can be modeled as the case in Figure 3(b) without losing particularity. The contact point P_3 now becomes the tangential point between the convex surface of the tail and the ground plane.

With $\mathbf{P}_1$ and $\mathbf{P}_2$ calculated from Eqs.(1-3), the position vector of P_3 with respect to the body coordinates $\{x_b, y_b, z_b\}$ can now be determined by finding the tangential point between the convex surface of the tail and the plane that contains points P_1 and P_2. Assuming the equation of the convex surface in the body coordinate system is $F(x, y, z) = 0$, then the equations to obtain $\mathbf{P}_3$ can be formulated as follows:

$$\begin{cases} F(P_{3x}, P_{3y}, P_{3z}) = 0 & (5.1) \\ F_x(P_{3x}, P_{3y}, P_{3z})(P_{1x} - P_{3x}) + F_y(P_{3x}, P_{3y}, P_{3z})(P_{1y} - P_{3y}) + F_z(P_{3x}, P_{3y}, P_{3z})(P_{1z} - P_{3z}) = 0 & (5.2) \\ F_x(P_{3x}, P_{3y}, P_{3z})(P_{2x} - P_{3x}) + F_y(P_{3x}, P_{3y}, P_{3z})(P_{2y} - P_{3y}) + F_z(P_{3x}, P_{3y}, P_{3z})(P_{2z} - P_{3z}) = 0 & (5.3) \end{cases}$$

where P_{ix}, P_{iy}, P_{iz} are the three components of $\mathbf{P}_i$, with $i = 1,2,3$ and $\mathbf{P}_i = [P_{ix}, P_{iy}, P_{iz}]^{\mathrm{T}}$. F_x, F_y and F_z in Eq.(5.2) and Eq.(5.3) are the partial derivatives of $F(x, y, z)$ with respect to x, y, and z respectively. Eqs.(5.1-5.3) all have definite geometric meanings. Eq.(5.1) makes sure that P_3 is on the surface, while Eq.(5.2) and Eq.(5.3) indicate that the tangential plane at P_3 also passes through P_1 and P_2. With $\mathbf{P}_1$ and $\mathbf{P}_2$ known from

Eqs.(1-3), Eqs.(5.1-5.3) now become an equation system with only three unknowns P_{3x}, P_{3y}, P_{3z}, thus $\mathbf{P}_3$ is solvable.

Note that, the current IMPASS prototype has a partial spherical surface at its tail. However, $F(x, y, z) = 0$ can also be designed as other types convex surfaces such as hyperboloid of one sheet, paraboloid, etc. As long as the contact point is the tangential point between the surface and the ground plane, Eqs.(5.1-5.3) will be valid.

Finally, with $\mathbf{P}_1$, $\mathbf{P}_2$ and $\mathbf{P}_3$ obtained, the configuration of the ground plane relative to the body coordinate system is determined definitely. The three orthogonal unit vectors describing the orientation of the ground can be found as:

$$\begin{aligned}\mathbf{x}'_o &= (\mathbf{P}_1 - \mathbf{P}_2)/\|\mathbf{P}_1 - \mathbf{P}_2\| \\ \mathbf{z}'_o &= \mathbf{x}'_o \times (\mathbf{P}_2 - \mathbf{P}_3)/\|\mathbf{x}'_o \times (\mathbf{P}_2 - \mathbf{P}_3)\| \\ \mathbf{y}'_o &= \mathbf{z}'_o \times \mathbf{x}'_o\end{aligned} \tag{6}$$

The ground coordinate system $\{x_o, y_o, z_o\}$ has its origin at point P_2, so the homogeneous transformation matrix from the ground frame to the body frame is established as:

$$\mathbf{H}_B^O = \begin{bmatrix} \mathbf{x}'_o & \mathbf{y}'_o & \mathbf{z}'_o & \mathbf{P}_2 \\ 0 & 0 & 0 & 1 \end{bmatrix} \tag{7}$$

By taking the inverse of the matrix $\mathbf{H}_B^O$, the configuration of the body attached frame $\{x_b, y_b, z_b\}$ with respect to the ground fixed frame $\{x_o, y_o, z_o\}$ is obtained as:

$$\begin{aligned}\mathbf{H}_O^B = \left(\mathbf{H}_B^O\right)^{-1} &= \begin{bmatrix} \begin{bmatrix}\mathbf{x}'_o & \mathbf{y}'_o & \mathbf{z}'_o\end{bmatrix}^T & -\begin{bmatrix}\mathbf{x}'_o & \mathbf{y}'_o & \mathbf{z}'_o\end{bmatrix}^T \mathbf{P}_2 \\ \mathbf{0} & 1 \end{bmatrix} \\ &= \begin{bmatrix} \mathbf{x}_b & \mathbf{y}_b & \mathbf{z}_b & \mathbf{B} \\ 0 & 0 & 0 & 1 \end{bmatrix}\end{aligned} \tag{8}$$

Thus, the forward kinematics of IMPASS with two spokes and the tail in contact with the ground is formulated completely. With given joint displacements, i.e. θ, d_1 and d_2, the position and orientation of IMPASS' body with respect to the ground are obtained and represented with the homogeneous transformation matrix $\mathbf{H}_O^B$. Theoretically, it is possible that the forward kinematics has multiple solutions. Inspecting the kinematic model of IMPASS in Figure 2, the multiple solutions are due to the existence of multiple tangential points of the surface and the ground plane, i.e. the whole spherical surface at the tail can have two tangential points with the plane that passes line P_1P_2, resulting in two forward kinematics solutions. However, the additional solution can be easily eliminated because only the lower portion of the spherical surface is actual and the tangential point at the upper portion is imaginary in the actual model and unique solution will be derived.

The procedures discussed above not only solve the forward kinematics in the current topology of the robot with two spokes and the tail contacting the ground, but also can be expanded to include the configuration transformations of the robot when taking multiple steps. Technically, touch sensors can be mounted at the tips of all the spokes. Within the current topology of the robot, if an additional spoke touches the ground and the topology is about to change, then the new contact point is detected by the touch sensor, its position with respect to the body frame is calculated, and a new ground coordinate system with known configuration is established for the next topology. Repeating Eqs.(1-8), the information about the body's new configuration can be updated based on new joint displacements.

4. INVERSE KINEMATICS ANALYSIS

Inverse kinematics is the reverse development to forward kinematics in which the joint displacements are calculated based on the specified position and orientation of the robot's body. As discussed in Section 3, the body's configuration is contained in matrix $\mathbf{H}_O^B$ with $\mathbf{x}_b$, $\mathbf{y}_b$ and $\mathbf{z}_b$ representing the orientation and $\mathbf{B}$ the position. The complete form of $\mathbf{H}_O^B$ is presented as follows:

$$\mathbf{H}_O^B = \begin{bmatrix} x_{bx} & y_{bx} & z_{bx} & B_x \\ x_{by} & y_{by} & z_{by} & B_y \\ x_{bz} & y_{bz} & z_{bz} & B_z \\ 0 & 0 & 0 & 1 \end{bmatrix} \tag{9}$$

which is a 4 by 4 matrix with 16 components. The 12 components in the first three rows are functions of θ, d_1, d_2, P_{3x}, P_{3y} and P_{3z}; their detailed expressions are presented in Appendix.

A rigid free body in 3D space has 6 d.o.f totally. However, the robot's body in Figure 2 only has 2 d.o.f because of the kinematic constraints. Therefore, the specification of the body's configuration must be selective and not all 6 d.o.f can be specified arbitrarily. To illustrate this, assume $\mathbf{H}_O^B$ takes the following numerical form:

$$\mathbf{H}_O^B = \begin{bmatrix} h_{11} & h_{12} & h_{13} & h_{14} \\ h_{21} & h_{22} & h_{23} & h_{24} \\ h_{31} & h_{32} & h_{33} & h_{34} \\ 0 & 0 & 0 & 1 \end{bmatrix} \tag{10}$$

Then, among the 12 numbers in Eq.(9), only 2 numbers can be chosen as inputs.

The selection of the body's position and orientation is based on the actual requirements for the robot. It is not necessary to investigate all possible combinations of the 2 numbers out of the 12 candidates. Since IMPASS is expected to walk and steer on the ground, any two components from its position vector $\mathbf{B}$ or from the direction vector $\mathbf{y}_b$ can be utilized as the input variables. The advantage of these combinations is that, the two components from $\mathbf{B}$ can be used to control the projected position of the robot's body on x_oy_o plane (ground plane), y_oz_o plane or x_oz_o plane. Additionally, the two components from $\mathbf{y}_b$ can be used to control the heading angle of the robot projected to the ground or the pitch angle projected to y_oz_o plane.

Assume that h_{14} and h_{24} in Eq.(10) are chosen as the input variables, which correspond to B_x and B_y in Eq.(9). Then two equations are established as:

$$\begin{cases} B_x = h_{14} & (11.1) \\ B_y = h_{24} & (11.2) \end{cases}$$

Eqs.(11.1-11.2), Eqs.(5.1-5.3), and Eq.(4) or Eq.(4)* for two parallel contacting spokes or two skew contacting spokes, will associatively generate a system of 6 equations with respect to 6 unknowns: θ, d_1, d_2, P_{3x}, P_{3y} and P_{3z}. With θ, d_1 and d_2 obtained, the inverse kinematics problem is solved. Note that, other combinations of h_{ij} can also be used to solve for θ, d_1, d_2 and the procedures are the same as above.

5. NUMERICAL SOLUTIONS

An example based on numerical simulations is presented in this section as a validation to the development in Section 3 and 4. The equations are solved using the embedded algorithm in *Mathematica* and the solutions are plotted.

Firstly, the basic geometric parameters of the IMPASS model are listed in the following table.

Table 1 Basic geometric parameters of IMPASS

Length of the axle l	16 (in)
Center of the spherical surface with respect to $\{x_b, y_b, z_b\}$	[0, -35, 14] (in)
Radius of the spherical surface	21 (in)
Total length of a spoke	23.5 (in)

And the joint displacements are chosen as: θ = 0.5 (rad), d_1 = 14 (in) and d_2 = 10 (in).

Applying Eqs.(1-5), the solutions to the tangential and contact point P_3 are:

[-4.709,-37.004,-6.367] and [3.637,-15.124,19.720]

The second solution can be eliminated because it corresponds to a tangential point at the upper portion of the spherical surface. Using Eqs.(6-8), the matrix $\mathbf{H}_O^B$ is determined now as:

$$\mathbf{H}_O^B = \begin{bmatrix} 0.970 & -0.116 & -0.213 & 5.336 \\ 0.093 & 0.989 & -0.119 & 4.438 \\ 0.224 & 0.095 & 0.970 & 10.762 \\ 0 & 0 & 0 & 1 \end{bmatrix} \quad (12)$$

Using the values contained in Eq.(12), the configuration of the IMPASS model is plotted in Figure 4. Note that in this figure, the partial spherical surface at IMPASS' tail is represented with a complete transparent sphere. This is just to illustrate the reason why the additional solution can be eliminated.

Since $\mathbf{H}_O^B$ in Eq.(12) becomes a matrix with numbers calculated from the forward kinematics, its components can now be utilized to validate the formulation of inverse kinematics in Section 4. In the first simulation, assume h_{14} = 5.336 and h_{24} = 4.438 are the two input variables, then using Eqs.(11.1-2) and Eqs. (5.1-5.3), the 4 solutions to the inverse kinematics problem are obtained and listed in Table 2.

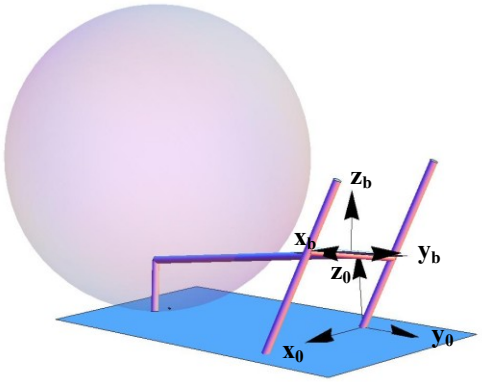

Figure 4 Forward kinematics solution

Table 2 Inverse kinematics solutions to the first simulation (h_{14} and h_{24} specified)

	Solution 1	Solution 2	Solution 3	Solution 4
θ	-2.881	1.827	0.5	2.076
d_1	14	14	14	14
d_2	10	10	10	10
P_{3x}	-4.709	4.709	-4.709	4.709
P_{3y}	-22.405	-14.752	-37.004	-22.390
P_{3z}	30.131	16.976	-6.367	-2.119

Apparently, Solution 3 matches exactly with the preset joint displacements. These solutions are plotted in Figure 5 to Figure 8.

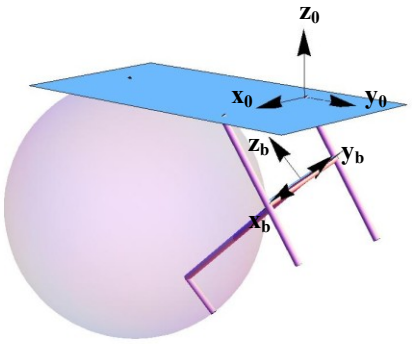

Figure 5 Solution 1 to the first inverse kinematics simulation

Inspecting Figure 5 to Figure 8, it is evident that if a criterion based on the effective range of the spherical surface and the joint displacements is applied, those unfeasible inverse kinematics solutions will be eliminated and only one feasible solution exists, which is no other than the current solution that matches with the preset joint variables.

In the second simulation, h_{12} = -0.116 and h_{22} = 0.989 are chosen as the two input variables and we are trying to control the direction of y_b axis. Applying Eqs.(11.1-2) and Eqs. (5.1-5.3) again, the 8 solutions to the inverse kinematics problem are obtained and listed in Table 3.

Table 3 Inverse kinematics solutions to the second simulation (h_{12} and h_{22} specified)

	Solution 1	Solution 2	Solution 3	Solution 4
θ	2.642	2.642	0.5	2.076
d_1	44.278	40.668	14	6.959
d_2	40.278	36.668	10	2.959
P_{3x}	-4.709	-4.250	-4.709	-4.250
P_{3y}	-37.004	-32.996	-37.004	-32.996
P_{3z}	34.367	34.467	-6.367	-6.467

	Solution 5	Solution 6	Solution 7	Solution 8
θ	2.642	2.642	0.5	0.5
d_1	-2.551	-11.211	-32.829	-44.921
d_2	-6.551	-15.211	-36.829	-48.921
P_{3x}	4.709	4.250	4.709	4.250
P_{3y}	-32.996	-32.004	32.996	-37.004
P_{3z}	-6.367	-6.467	34.367	34.467

Again, among the 8 solutions, solution 3 matches exactly with the preset joint displacements. These 8 solutions are plotted in Figure 9 to Figure 16.

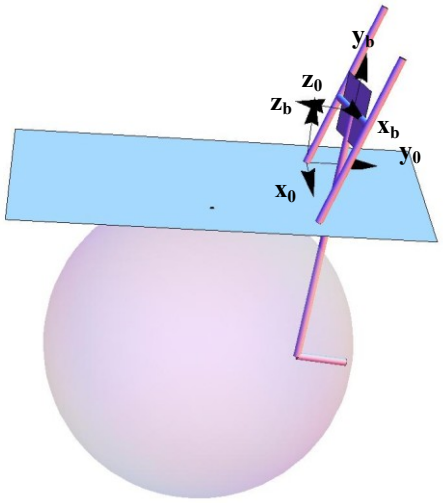

Figure 6 Solution 2 to the first inverse kinematics simulation

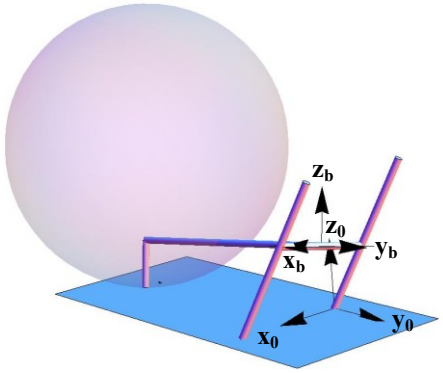

Figure 7 Solution 3 to the first inverse kinematics simulation

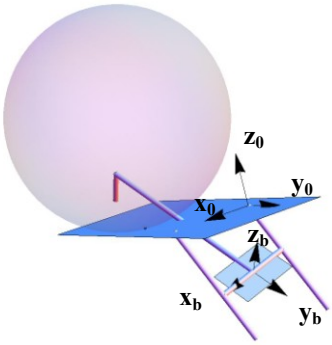

Figure 8 Solution 4 to the first inverse kinematics simulation

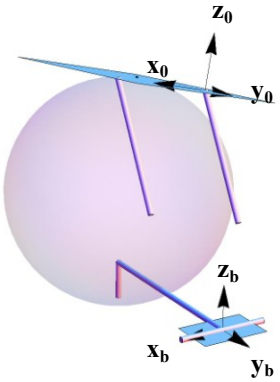

Figure 9 Solution 1 to the second inverse kinematics simulation

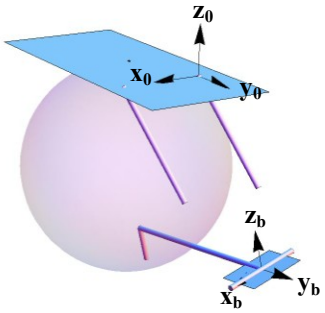

Figure 10 Solution 2 to the second inverse kinematics simulation

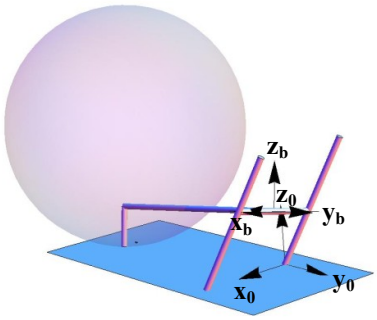

Figure 11 Solution 3 to the second inverse kinematics simulation

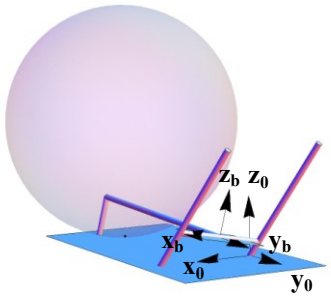

Figure 12 Solution 4 to the second inverse kinematics simulation

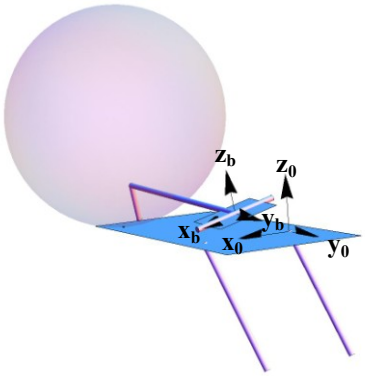

Figure 13 Solution 5 to the second inverse kinematics simulation

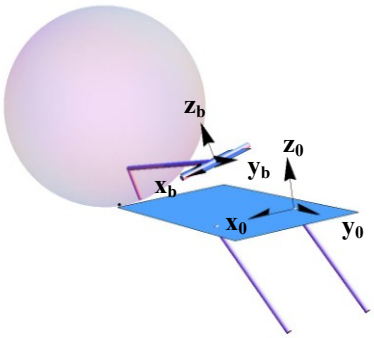

Figure 14 Solution 6 to the second inverse kinematics simulation

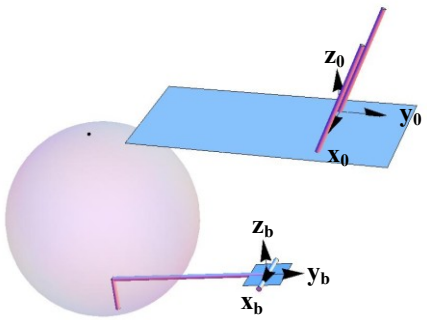

Figure 15 Solution 7 to the second inverse kinematics simulation

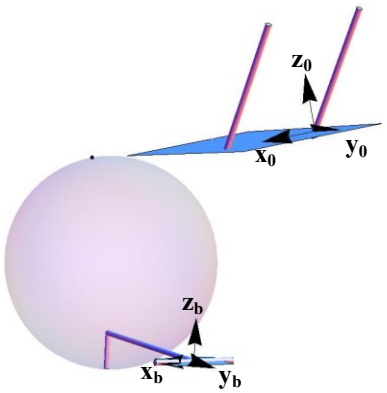

Figure 16 Solution 8 to the second inverse kinematics simulation

Inspecting Figure 9 to Figure 16, if a criterion based on the effective range of the spherical surface and the joint displacements is applied, the 6 unfeasible inverse kinematics solutions will be eliminated. However, in this case, solution 3 and 4 are both feasible solutions, if one solution needs to be eliminated, then more information of the body's configuration should be given.

6. CONCLUSIONS AND FUTURE RESEARCH

This paper presented the forward and inverse displacement analyses for the topology of IMPASS with two spokes and the tail contacting the ground. The formulation of the equations is validated with numerical simulations. For this particular case, the forward kinematics can reach unique solution. However, the inverse kinematics usually results in multiple solutions for this case. An elimination criterion based on the effective region of the spherical surface and the range of the joint displacements can be used to discard those unfeasible solutions. But to reach a unique solution, additional information about the configuration of the robot's body must be given.

The forward kinematics lays the theoretical foundation for the remote monitoring of IMPASS' motion on smooth terrains. And the inverse kinematics can assist in the motion planning of IMPASS to track any path. Besides these topics, the future research also include seeking the closed form solutions to the inverse kinematics to improve the computation efficiency and the design optimization of the surface geometry at the tail.

ACKNOWLEDGMENTS

The support of the National Science Foundation under Grant No. 0535012 is gratefully acknowledged. The authors would also like to thank Shawn Kimmel, J. Blake Jeans and the senior design teams from 2008 to 2009 for their contribution in the development of IMPASS prototypes.

REFERENCES

[1] Saranli, U., Buehler, M., and Koditschek, D.E. "RHex: A Simple and Highly Mobile Hexapod Robot," International Journal of Robotics Research 20, July 2001, pp. 616-631.

[2] Quinn, R.D., Nelson, G.M., Ritzmann, R.E., Bachmann, R.J., Kingsley, D.A., Offi, J.T. and Allen, T.J. (2003), "Parallel Strategies For Implementing Biological Principles Into Mobile Robots," International Journal of Robotics Research, Vol. 22 (3) pp. 169-186.

[3] Laney, D. and Hong, D.W.,"Kinematic Analysis of a Novel Rimless Wheel with Independently Actuated Spokes", 29th ASME Mechanisms and Robotics Conference, Long Beach, California, September 24-28, 2005.

[4] Laney, D. and Hong, D.W., "Three-Dimensional Kinematic Analysis of the Actuated Spoke Wheel Robot". 30th ASME Mechanisms and Robotics Conference, Philadelphia, Pennsylvania, September 10-13, 2006.

[5] Wang, Y., Ren, P., Hong, D., "Mobility and Geometrical Analysis of a Two Actuated Spoke Wheel Robot Modeled as a Mechanism with Variable Topology," 32nd ASME Mechanisms and Robotics Conference, Brooklyn, New York, August 3-6, 2008,

[6] Ren, P., Jeans, J.B., and Hong, D.W., "Kinematic Analysis and Experimental Verification on the Steering Characteristics of a Two Actuated Spoke Wheel Robot with a Tail," 33rd ASME Mechanisms and Robotics Conference, August 30 – September 2, 2009, San Diego, California, USA

[7] Ren, P., Wang, Y., Hong, D., "Three-dimensional Kinematic Analysis of a Two Actuated Spoke Wheel Robot Based on its Equivalency to A Serial Manipulator," 32nd ASME Mechanisms and Robotics Conference, Brooklyn, New York, August 3-6, 2008

[8] Tsai, L.-W., Robot Analysis: the Mechanics of Serial and Parallel Manipulators, John Wiley & Sons, Inc., 1999

APPENDIX

DETAILED EXPRESSIONS OF THE COMPONENTS IN EQ.(9)

$$\mathbf{H}_O^B = \begin{bmatrix} x_{bx} & y_{bx} & z_{bx} & B_x \\ x_{by} & y_{by} & z_{by} & B_y \\ x_{bz} & y_{bz} & z_{bz} & B_z \\ 0 & 0 & 0 & 1 \end{bmatrix} \tag{9}$$

For the case in which the two contacting spokes are parallel to each other, Eq.(4) is applied to eliminate d_1, Eqs.(1-3,6-8) are then implemented to derive the following expressions:

$$x_{bx} = \frac{l}{\sqrt{l^2+\Delta d^2}};$$

$$x_{by} = \frac{\Delta d\left(2ld_2 - l\Delta d - 2\Delta dP_{3x} + 2lP_{3z}\cos\theta + 2lP_{3y}\sin\theta\right)}{\sqrt{\left(l^2+\Delta d^2\right)\left[\left(-2lP_{3z} + \left(l\left(-2d_2+\Delta d\right)+2\Delta dP_{3x}\right)\cos\theta\right)^2 + \left(-2lP_{3y} + \left(l\left(-2d_2+\Delta d\right)+2\Delta dP_{3x}\right)\sin\theta\right)^2 + 4\Delta d^2\left(P_{3y}\cos\theta - P_{3z}\sin\theta\right)^2\right]}};$$

$$x_{bz} = \frac{2\Delta d\left(P_{3y}\cos\theta - P_{3z}\sin\theta\right)}{\sqrt{\left(-2lP_{3z} + \left(l\left(-2d_2+\Delta d\right)+2\Delta dP_{3x}\right)\cos\theta\right)^2 + \left(-2lP_{3y} + \left(l\left(-2d_2+\Delta d\right)+2\Delta dP_{3x}\right)\sin\theta\right)^2 + 4\Delta d^2\left(P_{3y}\cos\theta - P_{3z}\sin\theta\right)^2}};$$

$$y_{bx} = \frac{\Delta d\sin\theta}{\sqrt{l^2+\Delta d^2}};$$

$$y_{by} = \frac{-2l^2\left(P_{3y} + d_2\sin\theta\right) + \Delta d\left(-2\Delta dP_{3y}\cos^2\theta + l\left(l+2P_{3x}\right)\sin\theta + \Delta dP_{3z}\sin 2\theta\right)}{\sqrt{\left(l^2+\Delta d^2\right)\left[\left(-2lP_{3z} + \left(l\left(-2d_2+\Delta d\right)+2\Delta dP_{3x}\right)\cos\theta\right)^2 + \left(-2lP_{3y} + \left(l\left(-2d_2+\Delta d\right)+2\Delta dP_{3x}\right)\sin\theta\right)^2 + 4\Delta d^2\left(P_{3y}\cos\theta - P_{3z}\sin\theta\right)^2\right]}};$$

$$y_{bz} = \frac{2lP_{3z} + (2ld_2 - l\Delta d - 2\Delta dP_{3x})\cos\theta}{\sqrt{(-2lP_{3z} + (l(-2d_2+\Delta d)+2\Delta dP_{3x})\cos\theta)^2 + (-2lP_{3y} + (l(-2d_2+\Delta d)+2\Delta dP_{3x})\sin\theta)^2 + 4\Delta d^2(P_{3y}\cos\theta - P_{3z}\sin\theta)^2}};$$

$$z_{bx} = \frac{\Delta d\cos\theta}{\sqrt{l^2+\Delta d^2}};$$

$$z_{by} = \frac{l(l(-2d_2+\Delta d)+2\Delta dP_{3x})\cos\theta - 2P_{3z}(l^2+\Delta d^2\sin^2\theta) + \Delta d^2 P_{3y}\sin 2\theta}{\sqrt{(l^2+\Delta d^2)((-2lP_{3z} + (l(-2d_2+\Delta d)+2\Delta dP_{3x})\cos\theta)^2 + (-2lP_{3y} + (l(-2d_2+\Delta d)+2\Delta dP_{3x})\sin\theta)^2 + 4\Delta d^2(P_{3y}\cos\theta - P_{3z}\sin\theta)^2)}};$$

$$z_{bz} = \frac{-2lP_{3y} + (l(-2d_2+\Delta d)+2\Delta dP_{3x})\sin\theta}{\sqrt{(-2lP_{3z} + (l(-2d_2+\Delta d)+2\Delta dP_{3x})\cos\theta)^2 + (-2lP_{3y} + (l(-2d_2+\Delta d)+2\Delta dP_{3x})\sin\theta)^2 + 4\Delta d^2(P_{3y}\cos\theta - P_{3z}\sin\theta)^2}};$$

$$B_x = \frac{l^2 + 2d_2\Delta d}{2\sqrt{l^2+\Delta d^2}};$$

$$B_y = \frac{l(-2d_2+\Delta d)(2ld_2 - l\Delta d - 2\Delta dP_{3x} + 2lP_{3z}\cos\theta + 2lP_{3y}\sin\theta)}{2\sqrt{(l^2+\Delta d^2)((-2lP_{3z} + (l(-2d_2+\Delta d)+2\Delta dP_{3x})\cos\theta)^2 + (-2lP_{3y} + (l(-2d_2+\Delta d)+2\Delta dP_{3x})\sin\theta)^2 + 4\Delta d^2(P_{3y}\cos\theta - P_{3z}\sin\theta)^2)}};$$

$$B_z = -\frac{l(2d_2-\Delta d)(P_{3y}\cos\theta - P_{3z}\sin\theta)}{\sqrt{(-2lP_{3z} + (l(-2d_2+\Delta d)+2\Delta dP_{3x})\cos\theta)^2 + (-2lP_{3y} + (l(-2d_2+\Delta d)+2\Delta dP_{3x})\sin\theta)^2 + 4\Delta d^2(P_{3y}\cos\theta - P_{3z}\sin\theta)^2}}$$

When the two contacting spokes are skew and set 60 degrees apart from each other, Eqs.(1,2*,3,6-8) are implemented instead to derive the expressions in $\mathbf{H}_O^B$, these expressions have more complicated forms than the ones presented above, thus they are omitted due to the length requirement of the paper.